Identification of Heterogeneous Elastic Properties in Stenosed Arteries: a Numerical Plane Strain Study

Alexandre Franquet, Stéphane Avril, Pierre Badel, Rodolphe Le Riche

Identification of Heterogeneous Elastic Properties in Stenosed Arteries: a Numerical Plane Strain Study

ALEXANDRE FRANQUET[(1)], STÉPHANE AVRIL[(1)]*, RODOLPHE LE RICHE[(2)], PIERRE BADEL[(1)]

[(1)] *Ecole Nationale Supérieure des Mines de Saint Etienne ; Centre CIS ; Département D2BM-Biomatériaux et Biomécanique ; IFR IFRESIS 143 ; LCG -UMR CNRS 5146 ; 158 Cours Fauriel, 42023 Saint-Étienne Cedex 2, France*

[(2)] *Ecole Nationale Supérieure des Mines de Saint Etienne ; Institut Fayol, Département DEMO-Décision en Entreprise : Modélisation, Optimisation ; 158 Cours Fauriel, 42023 Saint-Étienne Cedex 2, France*

Abstract

Assessing the vulnerability of atherosclerotic plaques requires an accurate knowledge of the mechanical properties of the plaque constituents. It is possible to measure displacements *in vivo* inside a plaque using magnetic resonance imaging. An important issue is to solve the inverse problem that consists in estimating the elastic properties inside the plaque from measured displacements. This study focuses on the identifiability of elastic parameters *e.g.* on the compromise between identification time and identification accuracy. An idealised plane strain Finite Element (FE) model is used. The effects of the FE mesh, of the a priori assumptions about the constituents, of the measurement resolution and of the data noise are numerically investigated.

Keywords:

Finite element ; atherosclerosis ; inverse method ; identification ; elasticity ; artery

I. Introduction

Atherosclerosis is a disease where arteries are progressively obstructed, making blood circulation difficult. An atherosclerotic plaque composed essentially of lipids often forms into the artery wall at the arterial tree's bifurcations. It induces an inflammatory response and a local stiffening of the artery (Ross 1999). Ripping-off of atherosclerotic plaques in the carotid arteries is a major cause of mortality in OECD countries. The degree of luminal stenosis, corresponding to the artery's diameter reduction, is commonly used by physicians to decide an endarterectomy (a surgical intervention consisting in removing the plaque). NASCET and ECST studies have shown that patients with large stenosis (70% and more) benefit from carotid endarterectomy (NASCET steering comittee 1991; ECST collaborative group 1991). But it is more difficult to draw conclusions for patients with moderate stenosis. Moreover the phenomenon of artery remodelling makes this geometrical criterion alone insufficient (Casscells *et al.* 2003).

Studies have correlated the arterial compliance with the stroke risk (Kingwell *et al.* 2002). Cheng *et al.* (1993); Ohayon *et al.* (2001); Li *et al.* (2006); Trivedi *et al.* (2007) showed that the vulnerability of an atherosclerotic plaque can be assessed with a maximum stress

---

* Corresponding author: avril@emse.fr

criterion, which requires an accurate knowledge of the mechanical properties of the different plaque constituents. The estimation of these mechanical properties *in vivo* and the calculation of a stress criterion may be very valuable in helping physicians to evaluate the risk of imminent atherosclerotic plaque's ruptures.

Most of the time, the reconstruction of heterogeneous mechanical properties in arteries utilises Finite Element (FE) model updating (Chandran *et al.* 2003; Hamilton *et al.* 2005; Luo *et al.* 2006; Baldewsing *et al.* 2008; Le Floc'h *et al.* 2009).

An inverse problem is solved that consists in finding the parameters of a numerical model so that the predicted deformation fits experimental data (displacements or strains). It is currently not feasible to quantify true strain *in vivo*: arteries are stressed at their free state (Fung 1993; Rachev and Greenwald 2003; Ohayon *et al.* 2007) and their unstressed configuration cannot be assessed *in vivo*. However it is possible to obtain cyclic strains or displacements which are the strains or displacements measured between diastolic and systolic pressures. Ultrasound is one of the techniques that can be employed. De Korte *et al.* (1998) measured radial cyclic strains of a healthy artery thanks to Intravascular Ultrasonography (IVUS). Magnetic Resonance Imaging (MRI) is also a promising method. Draney *et al.* (2002) used a Magnetic Resonance phase contrast (PC-MRI) sequence to obtain radial cyclic strains *in vivo* of healthy arteries.

The *in vivo* identification of heterogeneous mechanical properties of diseased arteries has not been widely investigated in the literature. Baldewsing *et al.* (2008) worked with a 2D parametric finite element model. Elastic properties and contours of the different constituents are recovered one after another from IVUS data. Similarly Le Floc'h *et al.* (2009) created an integrated algorithm where both elastic properties and contours are identified at the same time from IVUS strain data. Computation time can then reach 24 hours for complex geometries.

Inasmuch as a lot of FE models are computed, the first approach to improve the identification time is to work on the FE models. The literature is very scarce on the propagation of errors through the FE mesh choice, besides the study of Le Floc'h (2009). Another approach is to reduce the number of unknown in the identification procedure. It is now well known that arteries are quasi-incompressible (Fung 1993; Black and Hastings 1998) and have a non linear behaviour (Fung 1993; Holzapfel and Weizsacker 1998; Holzapfel 2002; Pena *et al.* 2010). Baldewsing *et al.* (2008) and Le Floc'h *et al.* (2009) considered the mechanical behaviour to be linear elastic and supposed the Poisson's ratios to be known. Moreover the heterogeneities contours of atherosclerotic plaques, which are difficult to discern when data come from IVUS, can be distinguished with MRI (Auer *et al.* 2006; Li *et al.* 2006; Hermus *et al.* 2010).

The originality of this study is to numerically investigate the identifiability of the heterogeneities elastic parameters from simulated PC-MRI data (Draney *et al.* 2002). In particular, the effects of the FE mesh, of the a priori parameters values, of the data spatial resolution and of white noise corrupting experimental data are studied. The analysis focuses on the duration and the accuracy of the identification process.

II. Materials and methods

II.1. Finite Element Model

A cross section of an idealised atherosclerotic carotid artery has been modelled in 2D in a manner inspired by Li *et al.* (2008). Dimensions correspond to a 66% stenosis (see Figure 1). One node has been blocked in the $\vec{x}$ and $\vec{y}$ directions, and another has been blocked in the $\vec{y}$ direction to remove rigid body motion. A pressure of 5 kPa is applied uniformly onto the arterial wall, simulating the differential arterial pressure between diastole and systole (see Figure 2). Quasi-static conditions are assumed as the heart rate is approximately 1 Hz. The

mechanical behaviour is supposed to be linear elastic, under the hypothesis of plane strain. Three different materials are defined:

(1) Healthy tissue.

(2) A lipidic core composed essentially of fat.

(3) Diseased tissue including the fibrous cap and a part of the infected media, stiffer than the healthy tissue.

Hypotheses and assumptions of the numerical model are discussed in Section IV.

II.2. Reference data

Reference data serve as pseudo-experimental data. The behaviour of arteries is supposed to be quasi-incompressible. The elastic properties of the three materials are set to the following values:

(1) Healthy tissue: $E_{HT} = 600kPa$; $\nu_{HT} = 0.49$

(2) Lipidic core: $E_{LC} = 10kPa$; $\nu_{LC} = 0.49$

(3) Diseased tissue: $E_{DT} = 800kPa$; $\nu_{DT} = 0.49$

The reference data are the result of the computation of a FE model with about 130 000 CPE8H elements (hybrid plane strain quadratic quadrangular elements). This element allows to treat the hydrostatic pressure as an independent variable and is recommended for quasi-incompressible cases (ABAQUS 6.8 2008). The displacement field solution is then linearly interpolated on a regular grid of step S, which simulates a PC-MRI output with the voxel size S (see Figure 3) (Draney *et al.* 2002).

II.3. Inverse approach

An inverse approach consists in finding the parameters of a system, knowing its response. The principle is to minimise a distance J_2 (see Equation 1) with an optimisation algorithm.

$$\min_{\vec{\theta}} . J_2(\vec{\theta}) \tag{1}$$

where

$$J_2(\vec{\theta}) \ = \ \frac{1}{2} \sum_{i=0}^{N} (U_{reference}^i - u^i(\vec{\theta}))^2 \tag{2}$$

N : Number of interpolation nodes (grid nodes).

$(\vec{\theta})$: Vector of parameters, Young's moduli and Poisson's ratios depending on the test case considered (see Section II.4).

$u^i(\vec{\theta})$: Displacement from a FE simulation interpolated at the grid node *i.*

$U_{reference}^i$: Reference displacement at the grid node *i.*

A Levenberg-Marquardt algorithm with bounds handling (Marquardt 1963; Guyon and Le Riche 2000) is used to recover the elastic properties (see Figure 4). This algorithm needs gradients of $U_{x,y}^i$ with respect to $\vec{\theta}$ which are estimated by finite differences. Two termination criteria are set up:

$J_2(\vec{\theta}) \ \leq \ \varepsilon_a \ = \ 10^{-7}$: Accuracy on J_2 reached.

$\left\|\Delta\vec{\theta}\right\| \ \leq \ \varepsilon_b \ = \ 10^{-25}$: step $\left\|\Delta\vec{\theta}\right\|$ too small. No more improvement is expected.

The geometry of the FE model used is similar to the one used for generating reference displacement (see Figure 1). The displacements are always projected on the same grid as the reference data (see Figure 3(b)) and using the same procedure (see Section II.2).

II.4. Definition of numerical experiments

This section defines four series of tests which aim at studying the identifiability of mechanical properties. Starting from a default configuration (see Table 1), different parameters of the FE model and of the identification procedure are changed as explained hereafter. It is possible to measure the quality of an identification simply by comparing the identified mechanical properties (see Figure 4) to the target values defined in Section II.2. The total computation time is also observed. The influence of the FE mesh, the *a priori* Poisson's ratios, the grid' step size and the data noise are studied as explained hereafter.

II.4.1. Effect of the FE mesh

The first step is to choose appropriate meshes for subsequent tests. Two elements are tested: the CPE6 (plane strain quadratic triangular element, used in Le Floc'h (2009)) and the CPE8H. Four meshes made of 1000, 5000, 15000 and 40000 elements are investigated.

II.4.2. Effect of the a priori Poisson's ratios

As explained in Section I the Poisson's ratios are supposed to be known. However the choice of Poisson's ratios can have an influence on the Young's moduli identification. To study this sensitivity, Poisson's ratios are voluntarily unsettled during the identification procedure:

$$\{\upsilon_{HT},\upsilon_{LC},\upsilon_{DT},\} = \{\{0.45,0.45,0.45\},\{0.48,0.48,0.48\},\{0.49,0.49,0.49\}\{0.499,0.499,0.499\}\} \quad (3)$$

II.4.3. Effect of the grid step size

The grid step size is directly linked to the MRI spacial resolution. Current limitations of MRI devices are prone to affect the identification quality. The influence of MRI accuracy on Young's moduli recovery is investigated by interpolating the reference data on a regular grid of step sizes S taken as:

$$S = \{1\ mm, 0.5\ mm, 0.25\ mm, 0.125\ mm\} \quad (4)$$

II.4.4. Effect of a white Gaussian noise

The effect of a white Gaussian noise added to the reference data is studied because experimental data always contain noise. The reference displacements are defined as:

$$\overrightarrow{U^x_{reference}} = \overrightarrow{U^x_{reference}} + \sigma \text{ x } \overrightarrow{R_1} \quad (5)$$

$$\overrightarrow{U^y_{reference}} = \overrightarrow{U^y_{reference}} + \sigma \text{ x } \overrightarrow{R_2} \quad (6)$$

With:

$\sigma = 3\% \text{ x } \left\|\overrightarrow{U_{reference}}\right\|$: standard deviation

$\overrightarrow{R_1}$ and $\overrightarrow{R_2}$: random vectors following a standard normal law $N(0,I)$ where I is the $N_{interpolation\ nodes}$ x $N_{interpolation\ nodes}$ identity matrix.

A series of twenty different random noise vectors are added to the reference data in order to perform twenty different identifications. The default identification parameters are used except for the noise level (see Table 1). The mean and standard deviation of the errors on the identified values and the identification time are calculated.

III. Results

III.1. Effect of the FE mesh

Results are reported in Table 2. The identification with the CPE6 element always yields artery Young's moduli with an error lower than 2.4%. The errors of CPE8H identifications are always lower than 0.7% whatever the number of elements is. Five identifications terminated because sufficient accuracy on J_2 was reached (ε_a) and three terminated because of too small a step size (ε_b). It is remarkable that for low number of elements, the J_2 index has not reached the limit ε_a although the identification quality is still better than 2.4%.

This test leads to the selection of one mesh for each element type for the next numerical experiments. The best compromise between time and accuracy for the CPE8H element type is obtained for 5000 elements as explained hereafter. Concerning the CPE6 element type it appears that 15000 elements must be the best compromise. However we noticed that the algorithm reaches an accuracy of 1% after 346 seconds with 5000 elements (see Figure 5). Thus the two following meshes are selected as they are the best compromise between time and accuracy (see Figure 5):

❖ CPE6 5000: Although the accuracy on J_2 has not been reached, the algorithm finds a vector $\vec{\theta}_{final}$ after only 346 seconds:

$$\vec{\theta}_{final} = \left\{ E_{HA} = 606\ kPa,\ E_{LC} = 9.99\ kPa,\ E_{DT} = 799\ kPa \right\}$$

❖ CPE8H 5000: The identification quality is good (<1% on all Young's moduli), and the identification total time (557 seconds) is the lowest among identifications which converged according to the J_2 stopping criterion ε_a. The identified Young's moduli are:

$$\vec{\theta}_{final} = \left\{ E_{HA} = 604\ kPa,\ E_{LC} = 10.04\ kPa,\ E_{DT} = 800\ kPa \right\}$$

III.2. Effect of the *a priori* Poisson's ratios

Results are reported in Table 3. Poisson's ratios of 0.45 lead to errors of + 8% on the healthy artery Young's modulus, and a + 80% overestimation on the lipidic core Young's modulus for both meshes, whereas Poisson's ratios of 0.48 lead to errors of respectively + 5% and + 37%. Poisson's ratios of 0.499 significantly reduce E_{HA} (-35%) and E_{LC} (-87%).

III.3. Effect of the grid step size

The tests involving different grid step sizes are reported in Table 4. The results are very similar in terms of accuracy for the two types of elements. With the larger step size (1 mm), the error on the healthy artery Young's modulus is 9% and the error on the lipidic core is 8%. The identification time decreases when the step size decreases (excepted for CPE6 / 0.125 mm which terminated with a different criterion, $\left\| \Delta\vec{\theta} \right\| \leq 10^{-25}$). Note that with a given step size, for instance 1 mm, the CPE6 identification is twice as fast as that with CPE8H elements.

III.4. Effect of white Gaussian noise

Results are reported in Table 5. Twenty identifications have been performed from the same default initial parameters (see Table 1) for the two meshes. Twenty random noise vectors were added to reference displacements. The added noise affects both element types in the same marginal way in terms of Young's moduli standard deviations (respectively 0.21%, 0.30%, 0.03%).

IV. Discussion

IV.1. Stopping criterion

To our knowledge the effects of the criteria (ε_a and ε_b) on the identification of artery's mechanical properties have never been investigated. Our trials show the relative significance of the J_2 value since an identification with a coarser mesh may have a high J_2 value leading to the same identification quality than using a finer mesh. The Figure 6 shows that the minimum of J_2 is found at the value $E_{lipidic\ core}$ = 10 kPa (which is the reference value for this parameter) irrespectively of the mesh while the minimum value of J_2 depends on the chosen mesh.

Here, both selected models have 5000 elements, which can be compared to the 1152 triangular elements of Kallel and Bertrand (1996), the 2000 quadrangular elements of Khalil *et al.* (2006), the 4100 triangular elements of Fehrenbach *et al.* (2006) and the 15000 quadratic triangular elements of Le Floc'h *et al.* (2009). We show that an appropriate choice of FE model can save a substantial amount of computation time. Indeed, a FE model with only 5000 quadratic triangular elements is sufficient to obtain an identification accuracy lower than 1% while the identification time is potentially three times as fast as the identification with a 15000 quadratic quadrangles model (considering a better choice of termination criterion). In our opinion it represents a good compromise between time and accuracy. A less stringent choice of threshold for the second termination criterion ε_b can significantly reduce the computation time when this criterion is predominant.

IV.2. Model assumptions

IV.2.1. Model geometry

Atherosclerotic plaques are classified in categories (Cai *et al.* 2002). The artery modelled is an idealised type IV-V diseased artery where a large lipid pool is surrounded by fibrotic tissue. It should be kept in mind that MRI can distinguish different constituents, and not directly the different mechanical properties. However here we assume that the MRI data would provide the segmentation as presented in Figure 1.

IV.2.2. Surrounding tissues

Carotid arteries are encircled by soft tissue. Liu *et al.* (2007) already worked on the impact of such media on the arterial wall strains and highlighted its crucial role. Le Floc'h (2009) also studied the influence of an elastic medium surrounding the artery on the mechanical properties identification. It does not have an influence in our case because we use reference data and similar FE models between the pseudo-experimentation and the computations for the identification. But surrounding tissues should be considered in practice.

IV.2.3. Constitutive law

Even though the behaviour of arteries is known to be non-linear (for example Holzapfel (2002)), Khalil *et al.* (2006) underlined that the incompressible linear elastic stress-strain constitutive relations under isotropic and plane-strain assumptions are sufficient to model the behaviour of soft tissue undergoing small and quasi-static deformations. Moreover, Chabanas *et al.* (2004) pointed out that linear elasticity is acceptable for FE simulations of soft human tissue in the physiological range of pressure. The constitutive law chosen in this study is a linear approximation of the stress and strain variations in the diastole to systole range of loading. The elastic parameters can be interpreted as tangent moduli.

IV.2.4. Quasi-incompressibility

In this problem the Poisson's ratios are unknown as are the Young's moduli. Our results (see Section III.2) show that a bad estimation of the Poisson's ratio has a major influence on the identification quality in particular for the lipidic core whereas the Young's moduli of the healthy artery and of the diseased tissue are mainly affected in the case of an overestimation of the Poisson's ratios. In Table 6 we compare the identification times and accuracies of

optimisations when Poisson's ratios are set to 0.49 (identification of the three Young's moduli) against the identification times and accuracies when Poisson's ratios are three additional parameters to identify (identification of six parameters). The identification of six parameters provides an accuracy below 0.07% on the Young's moduli and below 0.35% on the Poisson's ratios. This table highlights that it is possible to save about three times the identification time by setting the Poisson's ratios. The accuracy on the Young's moduli is then negligibly impacted (<1%). This means that in a more general case the estimation of the Poisson's ratios is a key point: either the Poisson's ratios are accurately known and can be set in the identification procedure or these ratios must be identified together with the Young's moduli at the expense of an additional computational cost.

Starting from an heterogeneous coronary artery model with similar mechanical hypothesis and two different materials (a diseased tissue and a lipidic core), Le Floc'h (2009) kept a Poisson's ratio set to 0.49 in his identification method, but modified the reference data by changing the diseased tissue Poisson's ratio. Surprisingly it appeared that the method overestimated the Young's modulus of the artery when the Poisson's ratio is overestimated in the numerical model. On the contrary, our study reveals that the algorithm tends to soften the healthy artery and the lipidic core to compensate an overestimation of Poisson's ratios and vice versa. Le Floc'h (2009) worked with a fully integrated method where heterogeneities contours are identified, while the present study keeps the contours fixed and focuses only on the identification issues. This could explain the difference.

IV.2.5. Pre stress

An initial stress is induced by the blood pressure. The lowest pressure encountered in arteries is approximately 80 mmHg which corresponds to 10.66 kPa. Ohayon *et al.* (2007) considered the stress at the lumen border to be zero at diastole. Residual stresses are present inside the artery at free state as it has been shown in Fung (1993); Rachev and Greenwald (2003); Ohayon *et al.* (2007). It is currently difficult to assess this stress *in vivo*, although Ohayon *et al.* (2005) mentioned a method to estimate the initial configuration of a patient's coronary artery. Not taking into account these pre stresses can have a major influence on the final deformed artery (Alastrue *et al.* 2010), but it does not affect the current work since numerical reference data are considered and only the tangent moduli are estimated.

IV.3. Origin and quality of data

The grid step size has no visible effect on the accuracy of the identified Young's moduli from the step size of 0.5 mm downwards. However, in an experimental context, data can be noisy and affect the identification procedure. A large amount of data may be the key to reduce the identification time and to improve the accuracy. The results reported in Table 4, although deprived of any noise, hint at this trend. White Gaussian noise added to the reference data does not affect the identification time nor accuracy. Note that it is difficult to define a noise -3% here- which reflects a real experimental noise as we work with displacements as opposed to measures such as pixel intensity.

V. Conclusion

In this study, we have modelled an idealised plane strain atherosclerotic carotid artery with three different materials and have identified its tangent elastic properties with a Levenberg-Marquardt algorithm. We focused on how the numerical implementation affects identifiability of the Young's moduli where the identifiability describes here the compromise between moduli accuracy and computation time.The effects of the FE mesh refinement, of the Poisson's ratios, of data resolution, and of noisy data have been studied.

A FE model of 5000 quadratic triangular elements was shown to be sufficient for reaching an accuracy of 1% on the identified Young's moduli, although a finer mesh will better reflect the analytical displacements.

This leads to a second result: the classical index J_2 used in optimisation strategies depends on the mesh choice and should not be the only identification criterion. A second termination criterion corresponding to the change of mechanical properties between consecutive iterations is necessary to allow, in conjunction with a light FE mesh, a reduced computation time.

Our results also emphasize the importance of a correct estimation of the Poisson's ratios which can significantly alter the results.

This study mainly addressed errors arising from the model and from the inversion method. Another source of difficulties is the experimental data and its simulation which has been questioned by superimposing white Gaussian noise onto the reference displacements. Future work will focus on obtaining more realistic data by simulating a real MRI output and finally by working on real experimental data.

Acknowledgements

References

[1] ABAQUS 6.8. 2008. Abaqus Theory Manual. Dassault Systèmes Simulia Corp. Providence (RI,USA).

[2] Alastrue V, Garcia A, Pena E, Rodrigez JF, Martinez MA, Doblare M. 2010. Numerical framework for patient-specific computational modelling of vascular tissue. Int. J. Numer. Meth. Biomed. Eng. 26(1):35-51.

[3] Auer M, Stollberger R, Regitnig P, Ebner F, Holzapfel GA. 2006. IEEE-Inst Electrical Electronics Engineers Inc; 3-D reconstruction of tissue components for atherosclerotic human arteries using ex vivo highresolution MRI. IEEE T Med. Imaging 25(3):345-357.

[4] Baldewsing R, Danilouchkine M, Mastik F, Schaar J, Serruys P, van der Steen A. 2008. An Inverse Method for Imaging the Local Elasticity of Atherosclerotic Coronary Plaques. IEEE T Inf. Technol. B 12(3):277-289.

[5] Black J, Hastings G. 1998. Handbook of Biomaterial Properties. Chapman & Hall.

[6] Cai J, Hatsukami T, Ferguson MS, R. Small NP, Yuan C. 2002. Classification of Human Carotid Atherosclerotic Lesions With In Vivo Multicontrast Magnetic Resonance Imaging. Circulation 106(11):1368-1373.

[7] Casscells W, Naghavi M, Willerson JT. 2003. Vulnerable Atherosclerotic Plaque: A Multifocal Disease. Circulation 107(16):2072-2075.

[8] Chabanas M, Payan Y, Marecaux C, Swider P, Boutault F. 2004. Comparison of linear and nonlinear soft tissue models with post-operative CT scan in maxillofacial surgery. http://hal.archivesouvertes.fr/hal-00081939_v1/.

[9] Chandran KB, Mun JH, Choi KK, Chen JS, Hamilton A, Nagaraj A, McPherson DD. 2003. A method for in-vivo analysis for regional arterial wall material property alterations with atherosclerosis: preliminary results. Med. Eng. Phys. 25(4):289-298.

[10] Cheng G, Loree HM, Kamm RD, Fishbein MC, Lee RT. 1993. Distribution of Circumferential Stress in Ruptured and Stable Atherosclerotic Lesions. Circulation 87(4):1179-1187.

[11] De Korte C, Cespedes E, van der Steen A, Pasterkamp G, Bom N. 1998. Intravascular ultrasound elastography: assessment and imaging of elastic properties of diseased arteries and vulnerable plaque. Eur. J. Ultrasound 7(3):219-224.

[12] Draney M, Herfkens R, Hugues T, Pelc N, Wedding K, Zarins C, Taylor C. 2002. Quantification of Vessel Wall Cyclic Strain Using Cine Phase Contrast Magnetic Resonance Imaging. Ann. Biomed. Eng. 30(8):1033-1045.

[13] ECST collaborative group. 1991. MRC European Carotid Surgery Trial: interim results for symptomatic patients with severe (70-99%) or with mild (0-29%) carotid stenosis. Lancet 337(8752):1235-1243.

[14] Fehrenbach J, Masmoudi M, Souchon R, Trompette P. 2006. Detection of small Inclusions by Elastography. Inverse Probl. 22(3):1055-1069.

[15] Fung Y. 1993. Biomechanics: Mechanical properties of living tissues (2nd Ed.). Springer-Verlag.

[16] Guyon F, Le Riche R. 2000. Least Squares Parameter Estimation and the Levenberg-Marquardt Algorithm: Deterministic Analysis, Sensitivities and Numerical Experiments. Institut National des Sciences Appliquées. Technical report.

[17] Hamilton A, Kim H, Nagaraj A, Mun J, Yan L, Roth S, McPherson D, Chandran K. 2005. Regional material property alterations in porcine femoral arteries with atheroma development. J. Biomech. 38(12):2354-2364.

[18] Hermus L, van Dam GM, Zeebregts CJ. 2010. Advanced Carotid Plaque Imaging. Eur J. Vasc. Endovasc. Surg. 39(2):125-133.

[19] Holzapfel G. 2002. Biomechanics of soft tissues with application to arterial walls, Mathematical and Computational Modeling of Biological Systems. Centre International de Mathématiques CIM. pp. 1-37.

[20] Holzapfel GA, Weizsacker HW. 1998. Biomechanical behavior of the arterial wall and its numerical characterization. Comput. Biol. Med. 28(4):377-392.

[21] Kallel F, Bertrand M. 1996. Tissue elasticity reconstruction using linear perturbation method. IEEE T Med. Imaging 15(3):299-313.

[22] Khalil AS, Bouma BE, Kaazempur Mofrad MR. 2006. A combined FEM/Genetic Algorithm for Vascular Soft Tissue Elasticity Estimation. Cardiovasc. Eng. 6(3):95-104.

[23] Kingwell BA, Waddell TK, Medley TL, Cameron JD, Dart A. 2002. Large artery stiffness predicts ischemic threshold in patients with coronary artery disease. J. Am. Coll. Cardiol. 40(4):773-779.

[24] Le Floc'h S. 2009. Modulographie vasculaire : Application à l'identi_cation in vivo du module de Young local des plaques d'athérosclérose (Vascular modulography: Application to the in vivo identification of the local Young moduli of atherosclerotic plaques).[PhD Thesis (in french)]. [Grenoble (France)]: Université Joseph Fourier.

[25] Le Floc'h S, Ohayon J, Tracqui P, Finet G, Gharib AM, Maurice RL, Cloutier G, Pettigrew RI. 2009. Vulnerable Atherosclerotic Plaque Elasticity Reconstruction Based on a Segmentation-driven Optimization Procedure using Strain Measurements: Theoretical Framework. IEEE T Med. Imaging 28(7):1126-1137.

[26] Li ZY, Howarth S, Trivedi RA, U-King-Im JM, Graves MJ, Brown A, Wang LQ, Gillard JH. 2006. Stress analysis of carotid plaque rupture based on in vivo high resolution MRI. J. Biomech. 39(14):2611-2622.

[27] Li ZY, Tang T, U-King-Im J, Graves M, Sutcliffe M, Gillard J. 2008. Assessment of carotid plaque vulnerability using structural and geometrical determinants. Circ. J. 72(7):1092-1099.

[28] Liu Y, Dang C, Garcia M, Gregersen H, Kassab GS. 2007. Surrounding tissues affect the passive mechanics of the vessel wall: theory and experiment. Am. J. Physiol. Heart Circ. Physiol. 293(6):3290-3300.

[29] Luo J, Ying K, Bai J. 2006. Elasticity reconstruction for ultrasound elastography using a radial compression: An inverse approach. Ultrasonics 44(1):e195-e198.

[30] Marquardt D. 1963. An algorithm for least-squares estimation of nonlinear parameters. J. Soc. Ind. Appl. Math. 11(2):431-441.

[31] NASCET steering comitee. 1991. North American Symptomatic Carotid Endarterectomy Trial. Methods, patient characteristics, and progress. Stroke 22(6):711-720.

[32] Ohayon J, Dubreuil O, Tracqui P, Le Floc'h S, Rioufol G, Chalabreysse L, Thivolet F, Pettigrew R, Finet G. 2007. Influence of residual stress/strain on the biomechanical

stability of vulnerable coronary plaques: potential impact for evaluating the risk of plaque rupture. Am. J. Physiol. 293(3):1987-1996.

[33] Ohayon J, Finet G, Treyve F, Rioufol G, Dubreuil O. 2005 (vol. 1). A three-dimensional finite element analysis of stress 14 distribution in a coronary atherosclerotic plaque: *In-vivo* prediction of plaque rupture location, in: Biomechanics applied to computer assisted surgery. Vol. 1: Research Signpost, Trivandrum, INDE. pp. 225-241.

[34] Ohayon J, Teppaz P, Finet G, Rioufol G. 2001. *In-vivo* prediction of human coronary plaque rupture location using intravascular ultrasound and the finite element method. Coronary Artery Dis. 12(8):655-663.

[35] Pena E, Alastrue V, Laborda A, Martinez M, Doblare M. 2010. A constitutive formulation of vascular tissue mechanics including viscoelasticity and softening behaviour. J. Biomech. 43(5):984-989.

[36] Rachev A, Greenwald S. 2003. Residual strains in conduit arteries. J. Biomech. 36(5):661-670.

[37] Ross R. 1999. Atherosclerosis - An Inflammatory Disease. New Engl. J. Med. 340(2):115-126.

[38] Trivedi R, Li ZY, U-King-Im J, Graves M, Kirkpatrick P, Gillard J. 2007. Identifying vulnerable carotid plaques in vivo using high resolution magnetic resonance imaging-based FInite element analysis. J. Neurosurg. 107(3):536-542.

Figures
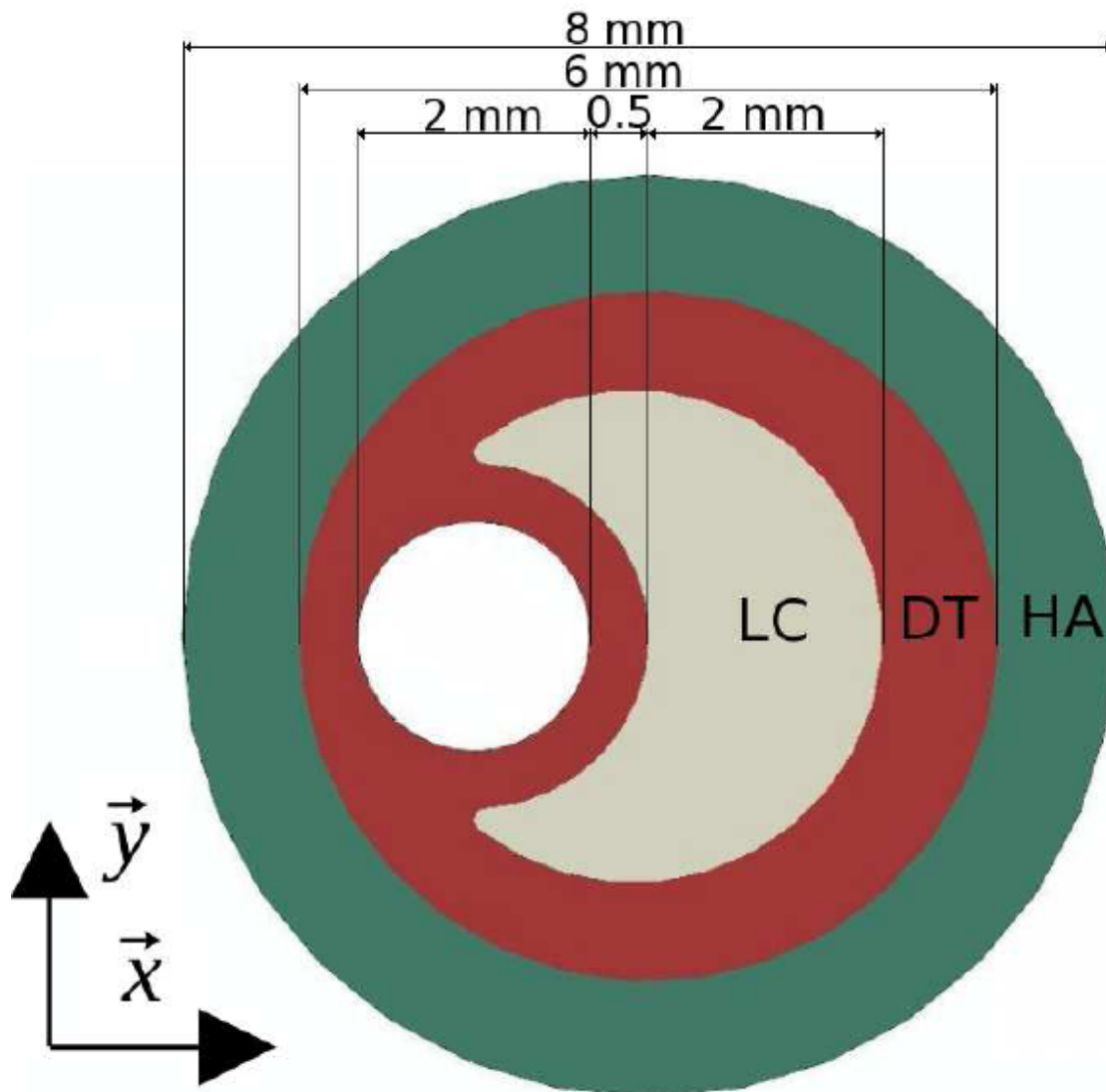
Figure 1: Dimensions and materials of the artery model. The lumen's initial shape is represented by the healthy artery (HA). Atherosclerosis induces some diseased tissue (DT) which modifies the blood circulation. The lipidic core (LC) is separated from the lumen by a fibrous cap included in the DT.
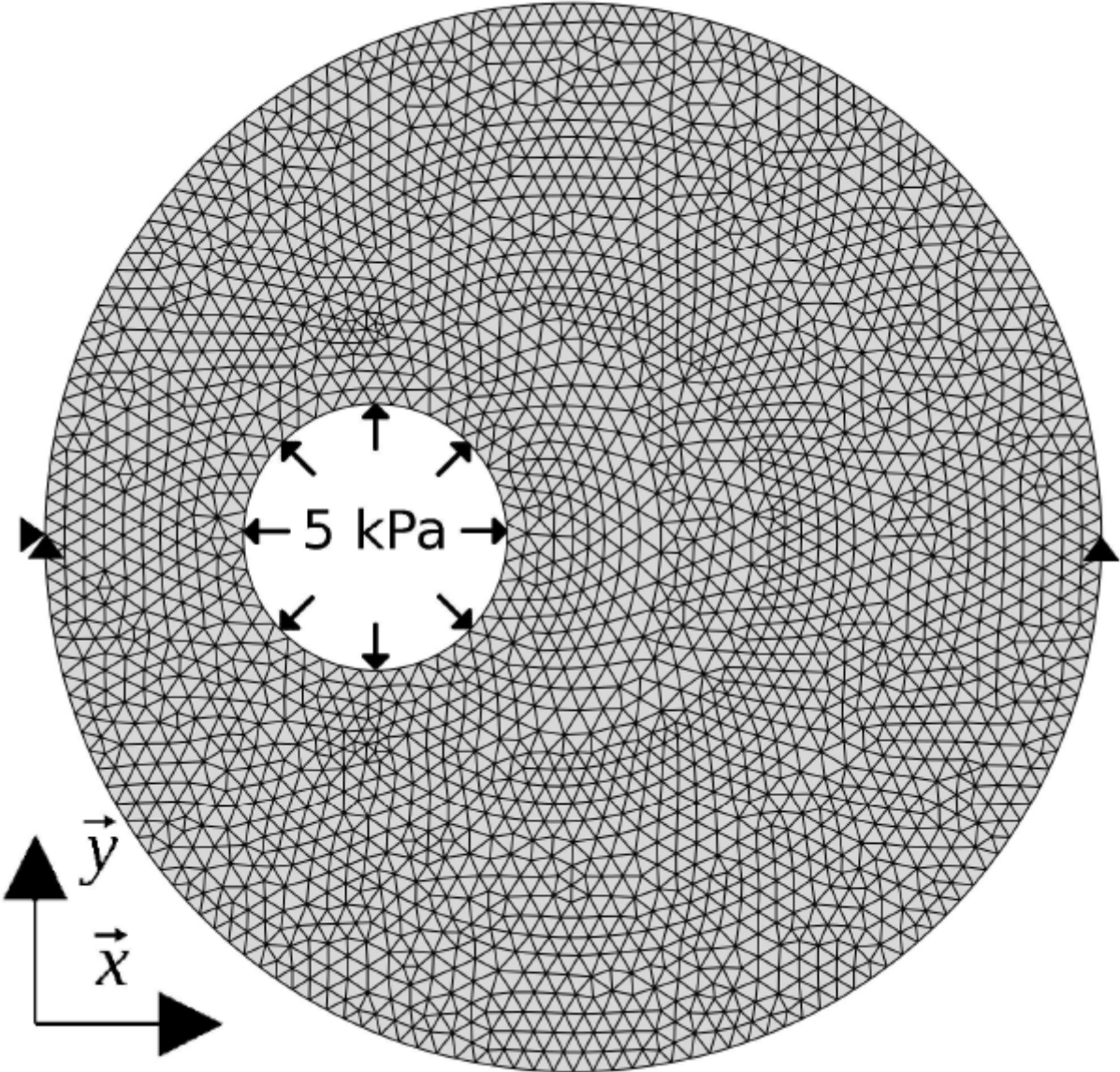
*Figure 2: Boundary conditions of the artery Finite Element model.*

(a)   (b)
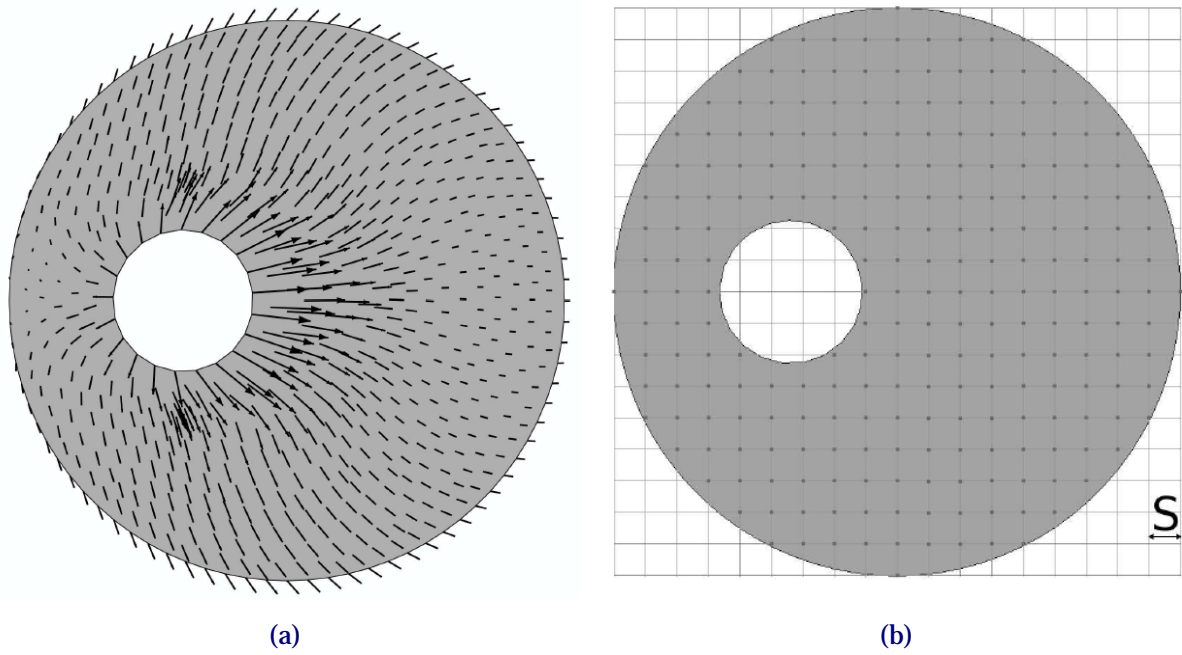
*Figure 3: Displacements from the FE computation (a) are linearly interpolated on the grid nodes (b). (a): Displacements at the nodes of the FE computation. (b): Interpolation grid with a voxel size S.*
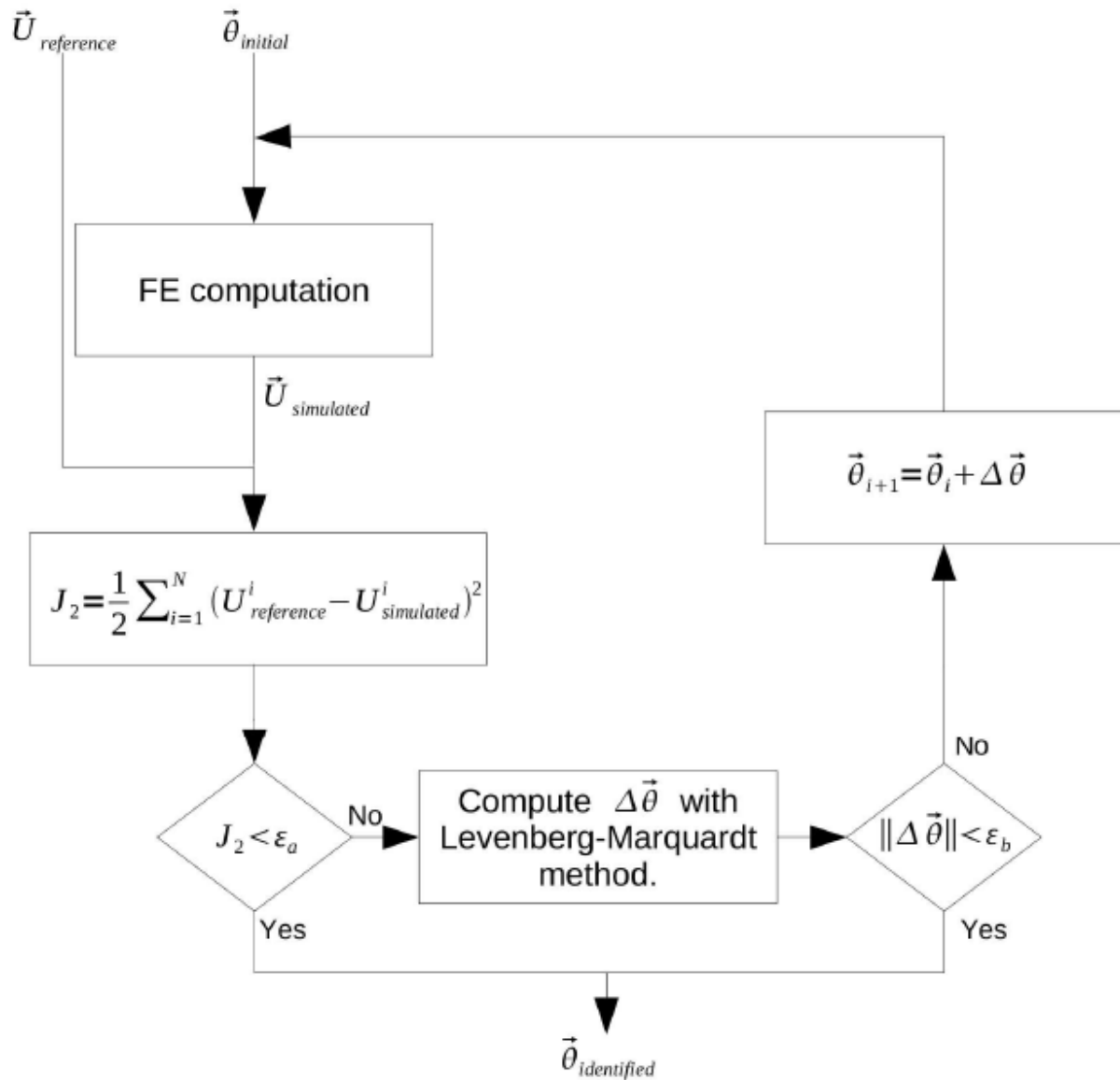
Figure 4: Flow chart of the inverse method.
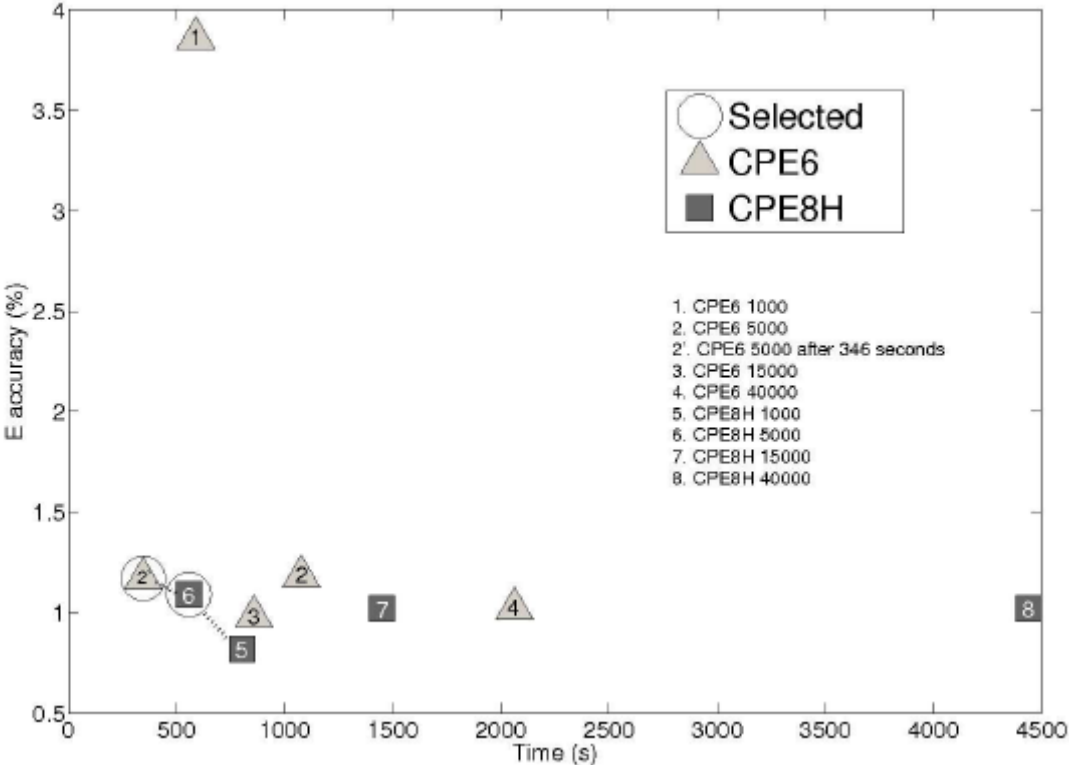
Figure 5: Pareto frontier accuracy/time for the different meshes. Accuracy is defined as the sum of the absolute values of errors on each Young's modulus.
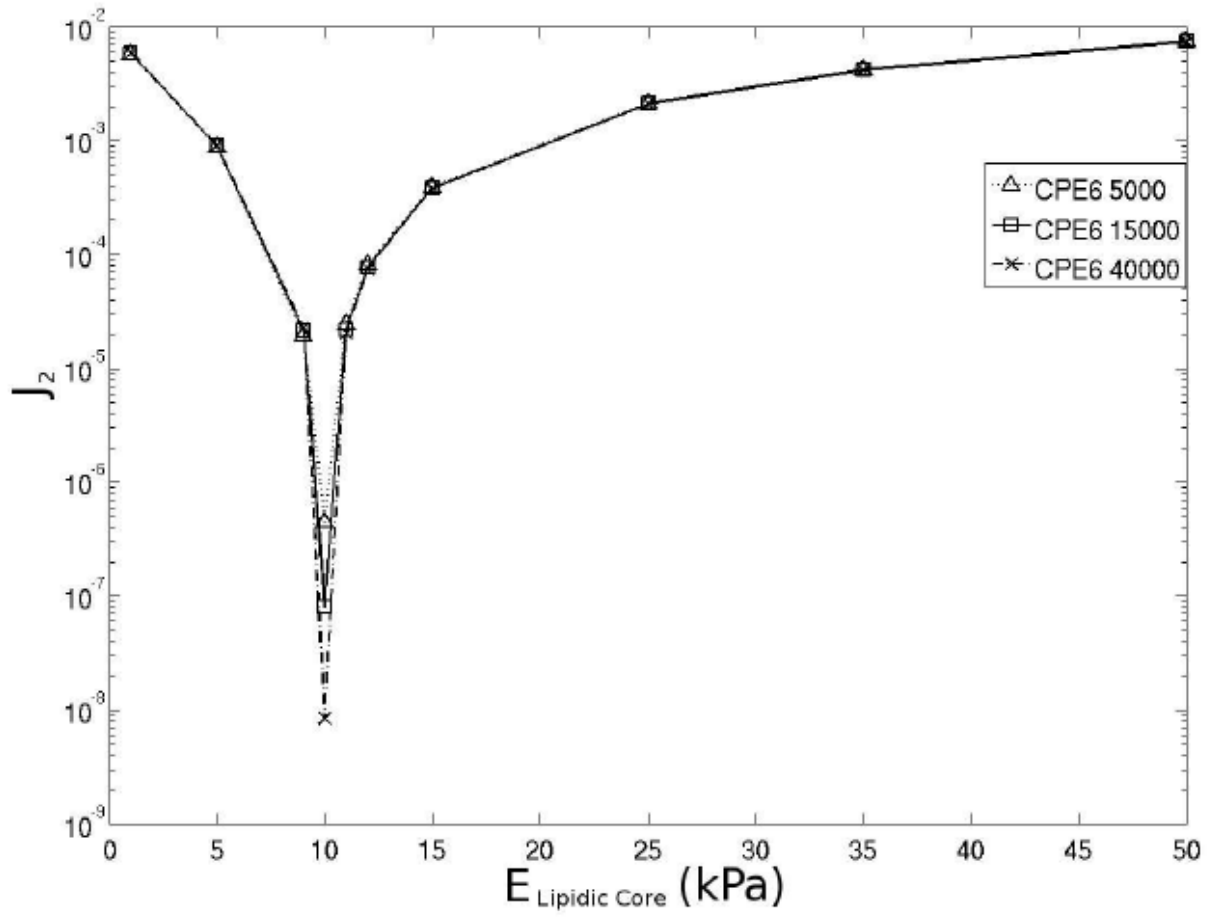
*Figure 6: J₂ criterion as a function of E$_{lipidic\ core}$ for a CPE6 mesh with 5000, 15000 or 40000
elements. Others mechanical properties are set to the reference values.*

Tables

Table 1: Default parameters

Initial vector of parameters	$\bar{\theta} = \{E_{HT} = 1000\ kPa,\ E_{LC} = 100\ kPa,\ E_{DT} = 1200\ kPa\}$
Mesh types	CPE6 5000 and CPE8H 5000
Set of Poisson ratios	$\{\upsilon_{HT}, \upsilon_{LC}, \upsilon_{DT},\} = \{0.49, 0.49, 0.49\}$
Grid step for the synthetic data	0.125 mm
Noise level added to synthetic data	0%

Table 2: Identification time and accuracy of optimisation procedures with respect to the size and the type of the FR mesh

Mesh type	E_{HA}	% E_{HA}	E_{LC}	% E_{LC}	E_{DT}	% E_{DT}	Time (s)		Termination
	(kPa)	(kPa)	(kPa)	(kPa)	(kPa)	(kPa)	1 FE	Total	criterion
References	600		10.00		800				
CPE6 1000	607	1.04%	9.77	-2.33%	798	-0.29%	0.38	590	$\left\|\Delta\vec{\theta}\right\| \leq 10^{-25}$
5000	603	0.55%	9.94	-0.56%	799	-0.07%	1.19	1038	$\left\|\Delta\vec{\theta}\right\| \leq 10^{-25}$
15000	604	0.68%	10.02	0.24%	799	-0.06%	3.99	858	$J_2(\vec{\theta}) \leq 10^{-7}$
40000	603	0.53%	10.04	0.44%	800	-0.05%	10.66	2063	$J_2(\vec{\theta}) \leq 10^{-7}$
CPE8H 1000	602	0.43%	9.97	-0.33%	800	-0.06%	0.84	803	$\left\|\Delta\vec{\theta}\right\| \leq 10^{-25}$
5000	604	0.64%	10.04	0.39%	800	-0.06%	3.83	557	$J_2(\vec{\theta}) \leq 10^{-7}$
15000	604	0.54%	10.04	0.43%	800	-0.05%	12.39	1149	$J_2(\vec{\theta}) \leq 10^{-7}$
40000	603	0.47%	10.05	0.51%	800	-0.04%	44.63	4440	$J_2(\vec{\theta}) \leq 10^{-7}$

Table 3: Identification time and accuracy of optimisation procedures when Poisson ratios are set to wrong values in the identification process.

Mesh type		υ_{HA}	υ_{LC}	υ_{DT}	E_{HA} (kPa)	% E_{HA} (kPa)	E_{LC} (kPa)	% E_{LC} (kPa)	E_{DT} (kPa)	% E_{DT} (kPa)	Total time (s)	Termination criterion
References		0.49	0.49	0.49	600		10.00		800			
CPE6	1000	0.45	0.45	0.45	650	8.26%	17.90	78.99%	804	0.45%	1017	$\left\|\Delta\vec{\theta}\right\| \leq 10^{-25}$
	5000	0.48	0.48	0.48	633	5.47%	13.65	36.48%	793	-0.87%	1002	$\left\|\Delta\vec{\theta}\right\| \leq 10^{-25}$
	15000	0.49	0.49	0.49	603	0.55%	9.94	-0.56%	799	-0.07%	1038	$\left\|\Delta\vec{\theta}\right\| \leq 10^{-25}$
	40000	0.499	0.499	0.499	394	-34.66%	1.23	-87.74%	844	5.53%	1187	$\left\|\Delta\vec{\theta}\right\| \leq 10^{-25}$
CPE8H	1000	0.45	0.45	0.45	648	8.03%	17.92	79.22%	804	0.47%	1579	$\left\|\Delta\vec{\theta}\right\| \leq 10^{-25}$
	5000	0.48	0.48	0.48	631	5.21%	13.69	36.88%	793	-0.84%	1620	$\left\|\Delta\vec{\theta}\right\| \leq 10^{-25}$
	15000	0.49	0.49	0.49	604	0.64%	10.04	0.39%	800	-0.06%	557	$J_2(\vec{\theta}) \leq 10^{-7}$
	40000	0.499	0.499	0.499	387	-35.43%	1.22	-87.82%	845	5.68%	2063	$\left\|\Delta\vec{\theta}\right\| \leq 10^{-25}$

Table 4: Identification time and accuracy of optimisation procedures when reference data are interpolated on grids with different steps sizes

Mesh type	S (mm)	E_{HA} (kPa)	% E_{HA} (kPa)	E_{LC} (kPa)	% E_{LC} (kPa)	E_{DT} (kPa)	% E_{DT} (kPa)	Total time (s)	Termination criterion
References		600		10.00		800			
CPE6 5000	1	655	9.12%	10.76	7.62%	795	-0.64%	462	$J_2(\vec{\theta}) \leq 10^{-7}$
	0.5	607	1.16%	10.01	0.11%	799	-0.12%	443	$J_2(\vec{\theta}) \leq 10^{-7}$
	0.25	606	1.04%	10.00	-0.01%	799	-0.11%	392	$J_2(\vec{\theta}) \leq 10^{-7}$
	0.125	603	0.55%	9.94	-0.56%	799	-0.07%	1038	$\left\| \Delta\vec{\theta} \right\| \leq 10^{-25}$
CPE8H 5000	1	654	8.99%	10.83	8.26%	795	-0.63%	802	$J_2(\vec{\theta}) \leq 10^{-7}$
	0.5	605	0.87%	10.83	0.65%	799	-0.07%	753	$J_2(\vec{\theta}) \leq 10^{-7}$
	0.25	604	0.74%	10.06	0.50%	799	-0.07%	653	$J_2(\vec{\theta}) \leq 10^{-7}$
	0.125	604	0.64%	10.05	0.39%	800	-0.06%	557	$J_2(\vec{\theta}) \leq 10^{-7}$

Table 5: Means and standard deviations of time and accuracy of twenty identifications for each mesh when 3% random Gaussian noise is added into the reference data.

Mesh type		E_{HA} (kPa)	% E_{HA} (kPa)	E_{LC} (kPa)	% E_{LC} (kPa)	E_{DT} (kPa)	% E_{DT} (kPa)	Total time (s)	Termination criterion
References		600		10.00		800			
CPE6 5000	Mean	603	0.52%	9.93	-0.65%	799	-0.08%	1114	$\left\| \Delta\vec{\theta} \right\| \leq 10^{-25}$
	Std. dev.	1.28	0.21%	0.03	0.26%	0.25	0.03%	48	
CPE8H 5000	Mean	601	0.17%	9.98	-0.20%	800	-0.03%	1768	$\left\| \Delta\vec{\theta} \right\| \leq 10^{-25}$
	Std. dev.	1.28	0.21%	0.03	0.26%	0.25	0.03%	61	

Table 6: Comparison between the identification time and accuracy of the optimisation procedures when the Poisson's ratios are set to 0.49 (3 parameters identification) or left as independent variables (6 parameters)

Mesh type	Number of parameters	E_{HA} (kPa)	% E_{HA} (kPa)	υ_{HA}	%υ_{HA}	E_{LC} (kPa)	% E_{LC} (kPa)	υ_{LC}	%υ_{LC}	E_{DT} (kPa)	% E_{DT} (kPa)	υ_{DT}	%υ_{DT}	Total time (s)	Termination criterion
References		600		0.49		10.00		0.49		800		0.49			
CPE6	3	603	0.55%	0.49	set	9.94	-0.56%	0.49	set	799	-0.07%	0.49	set	1038	$\left\|\Delta\vec{\theta}\right\| \leq 10^{-25}$
5000	3 (after 346s)	606	0.95%	0.49	set	9.99	-0.10%	0.49	set	799	-0.06%	0.49	set	346	
	6	600	0.07%	0.49	0.35%	9.95	-0.52%	0.49	0.01%	800	0.03%	0.49	-0.29%	1088	$J_2(\vec{\theta}) \leq 10^{-7}$
CPE8H	3	604	0.64%	0.49	set	10.04	0.39%	0.49	set	800	-0.06%	0.49	set	557	$J_2(\vec{\theta}) \leq 10^{-7}$
5000	6	600	0.03%	0.49	0.26%	10.00	0.01%	0.49	0.00%	800	0.05%	0.49	0.22%	1404	$J_2(\vec{\theta}) \leq 10^{-7}$